

## Chapter 2

# Systematically Understanding the Liquid Scintillation Counting Process: A Stochastic Computer Model

Philip J. Malcolm

*Biometry Section, Waite Agricultural Research Institute, Glen Osmond, South Australia 5064, Australia*

Philip E. Stanley

*Department of Clinical Pharmacology, The Queen Elizabeth Hospital, Woodville, South Australia 5011, Australia*

## INTRODUCTION

There exists a variety of methodological and computational techniques for estimating the true rate of nuclear disintegration from the rate observed using Liquid Scintillation Counting (LSC). There has, however, been no comprehensive approach treating the subject as a whole, and a very considerable knowledge and skill is therefore required to effectively utilise the full potential of the instrument.

We intended, in a project initiated in 1972, to provide just such a comprehensive approach. Especial attention was to be paid to setting up the instrument correctly in the first place, to gathering an appropriate amount of data and to accurately estimating the error distributions of the final estimates of the actual disintegration rate, especially for multi-labelled samples. It was felt that existing techniques could be blended into a single, comprehensive approach.

However, it soon became apparent that there was a reason why the many individually excellent but relatively limited approaches had been developed without the resultant emergence of a unified approach; this was because there were gaps in the scientific knowledge necessary for the development of a unified approach. While the LSC process is fundamentally based upon well-established laws of physics,<sup>1</sup> techniques for utilising the process tend to be based either upon a subset of the relevant laws (e.g. external standardisation<sup>2</sup>) or upon essentially empirical observations of the whole process (e.g. channels ratio<sup>3</sup>). There was at that time no published work dealing exhaustively and rigorously with the behaviour of the whole LSC process in terms of its fundamental components.

Thus, in adopting a unified approach, we continually found ourselves asking questions which could be answered definitively and rigorously only in special cases and not in the general case. The next step, therefore, was to develop an exhaustive and rigorous understanding of the whole LSC process in terms of its component processes. The obvious approach, that of computer simulation, was taken, with work beginning early in 1973. A very simple model, built to fix ideas, indicated that attention should first be

paid to processes occurring within the vial itself, and further that it was necessary, initially at least, to deal individually with each photon, rather than deal as a whole with all the photons arising from a particular event. This last conclusion was based upon an appreciation of the fundamentally discontinuous nature of the sequence of processes taking place within the cylindrical vial.

A model has since been built which details, on a photon by photon basis, the processes taking place within the solution and vial walls. The behaviour of the two photocathodes and the overall response of the detector chamber have also been modelled. The asymmetric and diverse nature of the vial cap and elevator platform has forced us to restrict attention to vials with 'perfectly' absorbing tops and bottoms; counting efficiency is somewhat reduced in practice by these absorbers. Detector response has not been modelled in detail first because of design variations between instruments and second because it is doubtful that the large amount of effort required would be adequately repaid in improved model performance. 'Background' counts have similarly been ignored because of their diverse and complicated origins.

The aim of this modelling project, namely to relate existing scientific knowledge, has nonetheless been satisfactorily fulfilled in that:

- (i) otherwise inaccessible empirical relationships, between primary- and secondary-emission photons for example, can now be readily ascertained;
- (ii) areas of possible improvement in instrument design are indicated; and
- (iii) a unified framework has been provided within which
  - (a) the workings of the instrument can be more easily understood, and
  - (b) its utilisation improved.

This chapter contains a general (non-mathematical) outline and discussion of the model, and also the main theoretical thrust of its results (items (i) and (iii a) above). The following chapter<sup>4</sup> deals with the more practical aspects of this modelling project and also discusses improvements in methodology resulting from it (item (iii) above). Item (ii) has been discussed elsewhere in a non-mathematical fashion,<sup>5</sup> wherein an optimised optical design is developed for an LSC system which is spherically – rather than cylindrically – symmetrical (as is the normal case). The logical design and mathematical details of the normal cylindrical model, the optimised design of the spherical system and a detailed model of the spherical system have been given in Refs. 6a and 6b.

As discussed elsewhere,<sup>7</sup> several other workers<sup>8-12</sup> have proposed fairly complete models of the LSC process, but none yet appear to have treated it rigorously in detail.

## OUTLINE OF THE NORMAL LSC PROCESS AS MODELLED

We restrict attention to binary scintillation systems, PPO and toluene, first because such systems have been thoroughly investigated by other workers and found to be well behaved and second because these systems are simpler and therefore more easily described mathematically. It is assumed that the scintillation system is excited only by low-energy  $\beta$ -emitting radioisotopes,  $^{14}\text{C}$  and  $^3\text{H}$  for example, first because samples including such radionuclides produce relatively few photons and are therefore particularly sensitive to colour and chemical quenching and second because  $\beta$ -particles from such sources have a path length which is negligible compared to vial radius (less than 0.5% for  $\beta$ -mean  $^{14}\text{C}$ , less than 0.2% for  $\beta$ -mean  $^3\text{H}$ <sup>13</sup>).

We assume that the radionuclide's  $\beta$ -spectrum follows the theoretical Fermi distribution,<sup>6a</sup> and also that nuclear disintegrations or  $\beta$ -events occur randomly within the volume of the scintillation solution, henceforth called solution. We also assume that only

one  $\beta$ -event is being processed by the LSC system at any one time, thereby restricting attention to samples whose activity is less than about  $2 \times 10^5$  disintegrations  $\text{min}^{-1}$ .

Nuclear disintegrations are therefore characterised by position and  $\beta$ -energy, position being uniformly random within the solution volume. The  $\beta$ -energy of any individual disintegration is also random in the sense that while it is unpredictable and independent of other  $\beta$ -events, the  $\beta$ -spectrum built up from a very large number of disintegrations follows the Fermi distribution for that isotope.

Such behaviour can be described mathematically at two different levels; at the *event* level in terms of the details of individual events; or alternatively at the *spectral* level whereupon the basic mathematical entity is a whole spectrum.<sup>1,2</sup> The event level was chosen for this work, first because many of the important processes in the normal cylindrical LSC system are fundamentally discontinuous (e.g. total internal reflection and secondary emission) and second because the mathematical form of the equations at the spectral level would be very complicated and intractable, and their dynamical behaviour could therefore be incomprehensible to the average LSC user.

A stochastic, probabilistic or Monte Carlo description at the event level has therefore been developed, individual  $\beta$ -events for example being characterised by generating:

- (i) an event position which is random three-dimensionally within the simulated solution; and
- (ii) a random  $\beta$ -energy within the range of the emitter, this being generated so that  $\beta$ -energies from a very large number of simulated events cumulatively follow the Fermi distribution characterising the observed  $\beta$ -spectrum.

Each  $\beta$ -event is therefore simulated individually, and the fate of each pseudo-photon arising from it is individually traced until either it generates a pseudo-photoelectron or it is absorbed and lost from the counting system. Variation in behaviour is achieved by randomly generating characteristics such as event position,  $\beta$ -energies, energies and escape directions of photons, etc. Such random behaviour is, however, constrained, either geometrically (e.g. a  $\beta$ -event must occur within the solution), or physically since spectra determining population behaviour are followed. A computer program is used to generate the required pseudo-random numbers, and, while these numbers are not 'perfectly' random, they are sufficiently so for the overall behaviour of the model to be independent of the pseudo-random number generator used.

Such a detailed stochastic simulation project assumes that there is effectively unlimited access to a large-scale computer. A Control Data 6400 computer was used for this work, and since individual simulation runs typically consumed several hours of central processor time, programs were usually loaded in the evening and then allowed to run until the following morning (the program occasionally monitors the computer's real-time clock, and, when necessary, automatically terminates itself just before the engineers begin daily maintenance at 7 a.m.).

A non-standard version of FORTRAN was chosen as the programming language, first because it is maintained in a reasonably reliable fashion by Control Data and second because reasonably efficient object code could be produced using a partially optimising compiler. It should be noted that a useful characteristic of the program was that machine or system errors occurring during its long period of execution usually resulted in its catastrophic termination, this situation being far preferable to them passing unnoticed.

But, to return to our central discussion, most ( $> 90\%$ ) of the  $\beta$ -energy released by a particular disintegration does not contribute to primary photon production by the scintillation system, but is lost from the counting process as low-grade heat energy.

Horrocks<sup>14</sup> has noted that the proportion of the  $\beta$ -energy contributing to primary photon production depends upon the  $\beta$ -energy  $E$ . This portion is known as the scintillation efficiency  $S_E$  and takes values of 0.024 for 0.5 keV up to 0.062 for energies in excess of 300 keV. Thus, if we let

$$E_p = S_E E$$

then  $E_p$  is the energy available for primary photon production. Impurity or chemical quenching lowers  $E_p$  still further, this being modelled by multiplying  $E_p$  by a fraction  $q$  where  $(1-q)$  is the portion of energy lost by impurity quenching.  $(1-q)$  is assumed to be independent of  $E$  and the energy conversion equation now becomes

$$E_p = qS_E E$$

Event position and  $E_p$  therefore characterise the disintegration in respect of light production and it must be noted that, even at this stage, several simplifying assumptions have been made in treating the system mathematically.

For example, Horrocks' data<sup>14</sup> relating scintillation efficiency and  $\beta$ -energy have been scaled to an  $S_E$  value of 0.052 for the average energy ( $\cong 50$  keV) of the  $^{14}\text{C}$   $\beta$ -spectrum,<sup>15</sup> but we require primary scintillation efficiencies (i.e. efficiency of production of primary photons) for monoenergetic sources. We require, for example, the primary scintillation efficiency for a monoenergetic 50 keV source rather than overall scintillation efficiency for  $\beta$ -energies *averaged* to 50 keV over the broad range of 0–156 keV for  $^{14}\text{C}$ . Monoenergetic data for primary photon production are unfortunately unavailable, so monoenergetic scintillation efficiencies calculated from averaged data must therefore be used.<sup>6a</sup> It has not been possible to correct these data for secondary and higher order emissions; use of a spherically symmetric instrument would, however, enable data to be corrected for secondary emission.<sup>6a, 6b</sup> The model is at this stage limited by the availability and accuracy of data, such as scintillation efficiencies, rather than a fundamental lack of theory (see the following chapter).

Other modelling constraints of a different flavour have also arisen, particularly with regard to the simulation of the detector apparatus and the simulation of the top and bottom of the vial. The optical properties of the vial shoulders and screw cap assembly, for example, are probably impossible to describe accurately mathematically because of their variable asymmetry and diffuse optical behaviour. We have therefore been forced to place a 'perfect' absorber above the scintillation solutions counted experimentally, this effect being quite easy to model.

Similarly, elevator platforms are in practice anything but perfect reflectors, and neither they nor vial bases are normally perfectly flat. Black photographic paper was therefore placed beneath the vial to act as a perfect absorber which was easily modelled. The paper was assumed not to contact the bottom of the vial, this last being taken to be perfectly flat. It was also assumed that the vials were perfectly cylindrical<sup>4</sup> and transparent, and that the refractive indices of the scintillation solution (1.502) and the vial glass (1.474 for Packard low background vials<sup>16</sup>) were identical, thus giving an optically continuous system; it should be noted that such assumptions, while invalid, give rise to relatively small errors.

The vials used in our counting experiments are compared with the simulated vial in Fig. 1. The height  $H$  of the solution was given a value of 4.0 cm in both the experiments and the model. (Note that it can therefore be assumed that photons can only escape to the detection chamber through the curved walls of the vial.)

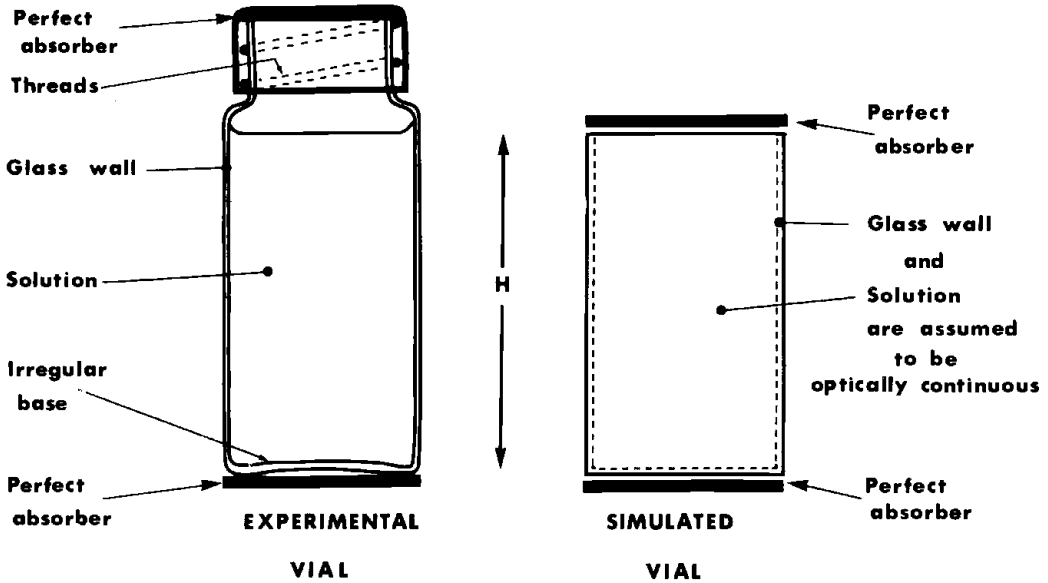


Fig. 1. Diagram comparing experimental and simulated vials.

Let us now consider photon production within the solution. We assume that excited fluor molecules emit photons in random directions three-dimensionally, and that these photons have random energies following the probability distribution given by the corrected fluorescence spectrum<sup>4</sup> of the fluor.

The energy  $E_p$ , calculated above, is available for primary photon production, and individual primary photons of randomised energies and escape directions are simulated until  $E_p$  is exhausted. As each photon has been characterised by energy and escape direction (relative to  $\beta$ -event position), its fate can now be determined as follows.

The absorption spectrum of the solution has been experimentally determined<sup>4</sup> and is used to calculate the absorption coefficient for a photon of that energy. This coefficient is used to generate a randomised distance  $x$  travelled through the solution by the photon. The distance  $y$  that it must travel in order to reach the curved sides of the vial is also calculated, whereupon:

- (i) if  $x \geq y$  and the photon approaches the vial's outer wall at an angle  $\psi$  less than the critical  $\psi_c$  in three dimensions, then it escapes towards the detector chamber;
- (ii) if  $x \geq y$  and  $\psi \geq \psi_c$ , then the photon will be totally internally reflected at the curved outer wall and can in theory never escape to the detection chamber.<sup>6a</sup> It will either
  - (a) escape through the top of the solution or the bottom of the vial, or
  - (b) be absorbed by the solution (since we assume that the vial walls are perfectly transparent);
- (iii) if  $x < y$ , then the photon will either
  - (a) be absorbed by the solution, or
  - (b) escape through the top of the solution or the bottom of the vial.

The photon has therefore three possible fates; first, escape to the detector chamber (which will be discussed shortly); second, escape through the top of the solution or the bottom of the vial whereupon it is absorbed and lost; or third, absorption by the sol-

ution, in which case it is either absorbed by a non-scintillating coloured agent and lost (colour quenching) or it is absorbed by the fluor, these two alternatives being simulated in a probabilistic fashion according to the relative absorption coefficient of the fluor at that photon's energy.

Should the fluor absorb a photon, then a secondary photon may be emitted with a probability given by the fluorescence quantum efficiency of the fluor (0.83 for PPO<sup>17</sup>). Should a secondary photon not be emitted, then the fluor has acted as a colour quenching agent in the usual fashion. The point at which the fluor absorbed the photon is calculated, and, as the fluor can be treated as point-source emitter, any secondary photons will be emitted at a known point in the solution.

Secondary photons can be simulated in a manner identical to primary photons since they are emitted from a known point in solution in a random direction three-dimensionally, and have a random energy following the fluorescence spectrum of the fluor (i.e. the energy of a photon emitted by a fluor molecule is independent of the energy of the photon absorbed by the molecule). Therefore, any photon, whether primary or secondary, will meet one of these fates: it is either

- (i) lost in the absorbers outside the top of the solution or the bottom of the vial;
- (ii) colour quenched in the usual fashion;
- (iii) colour quenched by the fluor;
- (iv) absorbed by a fluor molecule which subsequently emits a secondary photon; or
- (v) it escapes through the curved walls of the vial.

We have already discussed cases (i) to (iv), and will now consider (v). Having left the vial via its curved outer walls, a photon will either (a) pass through the narrow annular air gap between the top or bottom of the detector chamber and the vial, and therefore (vi) be lost from the counting process (see Fig. 2); or (b) it will enter the detector chamber of the instrument, whereupon

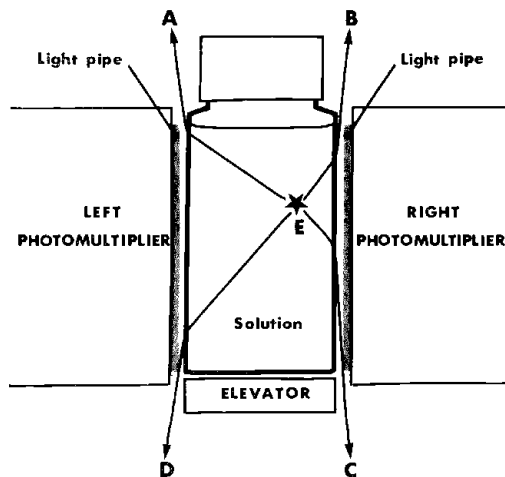


Fig. 2. A source of considerable light loss in the normal LSC instrument. Photons taking paths EA, EB, EC, ED will never enter the light pipe of the instrument illustrated, a Packard Model 3375 Tri-Carb system. They will instead be lost from the detector chamber. About 9% of the light leaving the vial is lost in a Packard 3375, this number being slightly larger for a Searle Isocap 300 instrument.

- (vii) it is absorbed in the detector (by the imperfect reflector for example);
- (viii) it passes through the photocathode of the photomultiplier without being absorbed or giving rise to a photoelectron;
- (ix) it gives rise to a photoelectron at the photocathode;
- (x) it is reflected back into the vial (see cases (i) to (v) above);
- (xi) it is reflected out of the detector chamber and lost from the counting process (case (vi) above); or
- (xii) it is reflected into the opposite side of the detector chamber (see cases (vii) to (xii)).

Consider first case (vi) above. One might expect that a negligibly small proportion of photons would escape through these annular air gaps since they are usually only about 1.0 mm wide. The authors have, however, demonstrated elsewhere<sup>6b, 7</sup> that these losses are disproportionately large because of the cylindrical symmetry of the standard counting vial, being about 9% for a solution 4.0 cm high in a Packard Model 3375 Tri-Carb system or a Searle Isocap 300 instrument.<sup>6b</sup>

Let us now consider the alternative case, that in which the photon enters the detector chamber, this last consisting usually of highly efficient mirrors which are designed to reflect light towards the photocathode of the appropriate photomultiplier (a portion of the light energy entering the photocathode is converted to photoelectrons; these are then amplified in the dynode chain of the photomultiplier and finally registered as an electrical pulse at the anode of the photomultiplier; the anode pulse is analysed by the remainder of the instrument to determine whether or not it arose from a valid 'count', i.e. resulted from an event of appropriate energy in the solution).

Now the design of the detector chamber and associated equipment varies markedly between instruments. For example, of the two instruments available for experimental use in this work, the detector chamber of one, an early model Packard Model 3375 Tri-Carb system, consisted of a rectilinear solid of 'lucite' or 'perspex' mirrored on the top, the bottom and the two sides perpendicular to the photocathodes, and containing a cylindrical hole down which the elevator moved bringing within it the vial. The detector of the other instrument, a Searle Isocap 300, consisted of a complicated curved mirror which was open to the photocathodes at each end and enclosed an air space containing the vial, the vial being loaded by an elevator moving down through circular holes in the top and bottom of the detector.

Because of this wide variation in detector design, and also because of the obvious difficulties in arriving at anything approaching an adequate mathematical description in even a special case, no attempt was made to describe in detail the path taken by photons after leaving the vial; instead, the overall response of the detector was assessed experimentally for light leaving different points on the vial's curved walls<sup>4</sup> (a vial covered completely with black photographic paper except for a small hole at various heights was loaded and counted out of coincidence, then rotated through a small horizontal angle and recounted, etc.; see appendix of Ref. 6a).

These data were then normalised in relation to the best response summed over both photomultipliers, and could thereby be used to determine the overall response of the detector chamber for *all* photons leaving a particular point on the vial's curved walls. Thus the fate of photons leaving the vial could be simulated in a probabilistic fashion according to the overall response of the detector for all photons leaving the vial at that point, with photons simulated as successfully reaching the photocathode giving rise to photoelectrons in a probabilistic fashion according to the photocathode quantum efficiency<sup>4</sup> for photons of that wavelength.

This approach to detector response was therefore adequate for cases (vii, viii, ix and xi) above, but inadequately accommodated case (x) (and therefore also for one possible result of case (xii)), since photons reflected back towards the especially blackened vial were absorbed by the black photographic paper covering almost all its surface. For photons leaving the vial at points midway between the two photomultipliers, this is a serious deficiency in the model since it may be crudely estimated that about 25% of the light leaving the vial is normally reflected back into it when using an early Packard Model 3375 Tri-Carb instrument, this portion being less with the Searle Isocap 300 instrument.

Thus, a photon emitted by the fluor must meet one of the fates described above; it is lost from the counting system in cases (i, ii, iii, vi, vii, viii and xi); it may eventually give rise to a photoelectron and thereby increase the probability of the parent disintegration being 'counted' in cases (iv and xii); it does give rise to a photoelectron in case (ix); and its behaviour is inadequately modelled in case (x) and, to a lesser extent, in case (xii).

The detailed response of the photomultipliers could not be modelled as there is insufficient data concerning pulse spread and losses, and summed photoelectron counts in each photomultiplier are therefore the significant output of the  $\beta$ -event simulated. These summed photoelectron counts were used to simulate coincidence thereby enabling the simulated counting efficiency to be assessed, and digital 'pulse-height spectra' of both the summed and lesser<sup>18,19</sup> kind to be accumulated.

## RESULTS AND DISCUSSION

The results presented herein are intended to give the reader some appreciation of the behaviour of the model of the LSC system, and several points in this connection must be mentioned immediately.

First, in validating the model, an extensive laboratory program was conducted<sup>4</sup> to provide the necessary calibration data, and also to provide experimental results with which the forecasts of the model could be compared. It will be shown here, and also in Chapter 3, that, by and large, the model faithfully reproduces the behaviour observed in practice, especially under the more normal quenching conditions.

This does not mean that the authors are suggesting that the model might in some way replace direct laboratory measurements of aspects of the LSC process. This would, in their opinion, currently be quite unrealistic because of the many simplifying assumptions made in defining the model, because some of the data included in the model are necessarily only approximate and also because of the probabilistic nature of the model (see below).

The role of this model is rather to complement and integrate knowledge obtained by direct experimentation. The model is not intended to specify in a completely rigorous numerical fashion the relationships constituting the LSC process. Thus, while the reader will discover many interesting numerical data in the following pages, these data have been presented in order to illustrate the qualitative, not the quantitative, relationships involved. Correspondingly, the main thrusts of our considerations will be the discussion of qualitative, not quantitative, relationships, and these discussions will generally serve to provide a practical background for, and interpretation of, the results produced by the model.

Before turning attention to the model's behaviour for actual  $\beta$ -emitters, let us first consider its behaviour for imaginary sources of monoenergetic  $\beta$ -particles. Table 1 illus-

trates the behaviour expected for unquenched solutions containing sources of monoenergetic (internal) electrons.

There are several points of immediate interest in Table 1(a). Clearly  $\beta$ -events of very low energy (e.g.  $< 1.5$  keV) will be difficult to measure because they emit so few primary photons (e.g.  $< \cong 15$ ). Some of this emitted energy will be lost by absorption, and of the photons reaching a (bialkali) photocathode, only about 27% will give rise to photoelectrons.

The importance of photocathode response for low  $\beta$ -energies can be appreciated by comparing results for lower pseudo-discriminator settings of a minimum of two and three photoelectrons. Indeed, in the development of LS spectrometers over the past two decades, the improvement of photomultiplier response has been an area of critical attention and considerable progress.<sup>20</sup>

The instrument's detection efficiency increases rapidly with  $\beta$ -energy because the portion of energy available for primary photon production increases rapidly with energy (see above). Quite respectable counting efficiencies are obtained for unquenched  $\beta$ -events

**Table 1 (a).** Simulation of monoenergetic internal  $\beta$ -emitters—comparison of  $^3\text{H}$  and  $^{14}\text{C}$   $\beta$ -spectra (unquenched sample).

$\beta$ -energy <sup>a</sup> $e$ (keV)	Total no. of primary photons produced	Percent counting efficiencies for a 'pulse' of at least $n$ photoelectrons		Portion of $\beta$ -spectrum of energy $\geq e$ keV	
		$n = 2$	$n = 3$	$^3\text{H}$	$^{14}\text{C}$
1.2	11	12.8	4.5	89.1	98.8
1.3	13	14.3	5.5	88.2	98.7
1.4	14	15.9	6.6	87.2	98.6
1.5	15	18.7	8.4	86.2	98.5
1.6	16	20.9	9.6	85.2	98.4
1.7	17	22.8	11.2	84.2	98.3
1.8	19	25.5	13.2	83.1	98.2
1.9	20	27.9	15.2	82.1	98.1
2.0	21	30.4	17.7	81.1	98.0
2.1	22	31.8	18.9	80.1	97.9
2.2	24	34.4	21.0	79.0	97.8
2.3	25	36.0	23.3	78.0	97.7
2.4	26	38.3	25.8	77.0	97.6
2.5	27	40.7	28.0	76.0	97.5
3.0	34	50.4	38.6	70.8	97.0
3.5	40	59.0	48.6	65.7	96.5
4.0	47	66.8	58.8	60.7	96.0
4.5	54	73.6	66.8	55.8	95.5
5.0	61	78.7	73.3	51.1	95.0
5.5	68	82.8	79.2	46.6	94.4
6.0	75	85.7	82.9	42.2	93.9
6.5	82	89.0	87.0	38.0	93.4
7.0	89	90.6	89.3	34.1	92.8
50	796	100	100	0	44.5
100	1683	100	100	0	8.3
500	9486	100	100	0	0

<sup>a</sup>10,000 events were simulated in each case.

of energy greater than say 7 keV, and events of even higher energy clearly produce so many primary photons that a counting efficiency of 100% is virtually guaranteed. It is also interesting to note that the lower pseudo-discriminator setting becomes less and less important as  $\beta$ -energy increases. This behaviour is of course to be expected.

The last two columns of Table 1(a) illustrate why samples containing  $^{14}\text{C}$  behave in practice differently to samples containing  $^3\text{H}$ . This is because  $^3\text{H}$  emits  $\beta$ -particles in a much lower energy range than  $^{14}\text{C}$ . Thus, according to Table 1(a), only about 34% of  $^3\text{H}$   $\beta$ -events are counted with an efficiency greater than 90%, and about 10% of  $^3\text{H}$  events fall into the very low ( $\cong 10\%$ ) efficiency range. About 90% of  $^{14}\text{C}$   $\beta$ -particles, by contrast, are counted with at least 90% efficiency, and only about 1% fall into the very low ( $\cong 10\%$ ) efficiency range.

These relationships are observed in the laboratory first in that, in an integral window, an unquenched  $^3\text{H}$  sample generally counts at about 60–65% efficiency, this by comparison with the efficiency of 95%+ normally expected with an unquenched  $^{14}\text{C}$  sample.

Second,  $^3\text{H}$  is much more sensitive to quenching than is  $^{14}\text{C}$ . This is to be expected since a relatively large proportion of  $^3\text{H}$  events occur in the very low energy range, and therefore give rise to very few primary photons. Thus, should even a few photons be lost by colour quenching, then quite marked decreases in counting efficiency will be observed; similarly, in the case of impurity or chemical quenching, even fewer primary photons are produced in the first place.

Table 1(b) serves to illustrate the probabilistic nature of the model's behaviour. Differing counting efficiencies were generated by simulation runs whose only difference lay in the sequence of pseudo-random numbers used to drive the model.

Note that the stochastic variation in results produced by the model might be thought to be analogous with the variation in laboratory results due to experimental error. It would, however, be dangerous to take this analogy too far; for example, while the distribution of experimental estimates of counting efficiencies is known to be Poissonian,

**Table 1 (b).** Simulation of monoenergetic internal  $\beta$ -emitters—showing the probabilistic behaviour of the model; comparison of results obtained using different sequences of pseudo-random numbers.

$\beta$ -energy <sup>a</sup> (keV)	Percent counting efficiencies for a pulse of at least $n$ photoelectrons (unquenched samples)			
	$n = 2$		$n = 3$	
	Sequence 1	Sequence 2	Sequence 1	Sequence 2
3.0	50.4	50.9	38.6	38.5
3.5	59.0	60.2	48.6	50.1
4.0	66.8	66.5	58.8	58.0
4.5	73.6	74.1	66.8	67.2
5.0	78.7	78.7	73.3	73.5
5.5	82.8	82.9	79.2	79.1
6.0	85.7	85.6	82.9	83.0
6.5	89.0	88.7	87.0	86.6
7.0	90.6	91.2	89.3	89.8
7.5	93.1	92.7	92.0	91.8

<sup>a</sup>10,000 events were simulated in each case.

the distribution of the model's predictions is unknown. The reader is therefore urged once again to use these results in a qualitative rather than quantitative fashion.

In turning now to models of actual  $\beta$ -emitters we will restrict attention to the Searle Isocap 300 instrument, this despite the fact that the Packard Model 3375 Tri-Carb system has been modelled to the same degree of detail. The reason for this restriction, namely the optical qualities of the perspex light pipe installed in our early model machine, is discussed in detail in the following chapter.

Tables 2(a) and (b) show in some detail how  $^3\text{H}$  and  $^{14}\text{C}$  behave under different conditions of chemical quenching. Tables 3(a) and (b) provide similar details for the colour quenching situation, and chemically- and colour-quenched simulation runs are compared in Table 4. Five thousand events were simulated in all the above cases.

As these results are entirely in accordance with what is to be expected we will not discuss them in detail; the reader is instead recommended to peruse them at leisure. But we will discuss some of the more interesting relationships between comparable simulation runs of chemically- and colour-quenched  $^3\text{H}$  and  $^{14}\text{C}$  samples. The samples considered are those whose behaviour is detailed in Table 4.

Figures 3 and 4 show how the degree of light trapping due to the curved walls of the vial varies for  $^3\text{H}$  and  $^{14}\text{C}$  under chemical- and colour-quenching conditions. It must be mentioned immediately that data have only been included for those events in which coincidence is enabled; and, in this case, the total number of total internal reflections (at the curved outer walls of the vial) for *all* photons generated in simulating the event was divided by the total number of photons leaving the vial via its curved walls.

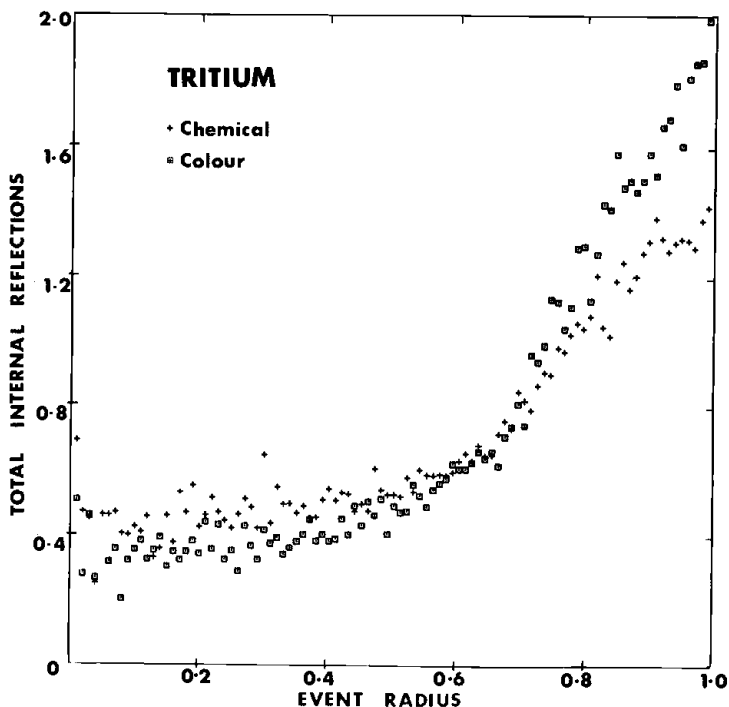


Fig. 3. Light trapping due to the curved walls of the counting vial as a function of the event radius (distance of event from the cylindrical axis) for colour- and chemically quenched  $^3\text{H}$  events.

Table 2 (a). Simulation of the unquenched and impurity quenched situations -  $^3\text{H}$ .

	Argon-purged $q^d = 0.9$		Air-quenched $q = 0.8$		Impurity quenched to equivalent of $30 \mu\text{l}$ of $\text{CCl}_4$ in a 20 ml sample $q = 0.5$	
	All events	Coincident events	All events	Coincident events	All events	Coincident events
Average $\beta$ -energy (keV)	5.6	7.4	5.6	7.5	5.8	8.3
Average number of primary photons	65	86	57	78	36	54
Average number of primary photons trapped due to cylindrical symmetry	23	30	20	27	13	18
Average number of secondary photons	44	57	38	51	24	35
Average number of photons colour quenched by PPO	8	11	7	10	5	7
lost in top absorber	9	12	8	11	5	7
lost in bottom absorber	10	13	8	12	5	8
leaving near side of vial	17	24	16	21	10	15
leaving far side of vial	18	24	15	23	10	15
lost in near side of detector	8	10	7	9	4	6
lost in far side of detector	9	13	8	12	5	8

reaching near photocathode <sup>a</sup>	9	13	8	12	6	9
reaching far photocathode <sup>b</sup>	9	12	8	11	5	7
Average number of photoelectrons in near photomultiplier	2	3	2	3	1	2
in far photomultiplier	2	3	2	3	1	2
Average summed 'pulse height'	4	6	3	6	2	4
Average lesser 'pulse height'	1	2	1	2	0	1
Proportion of photons reaching detector after $m$ re-emissions						
$m = 0$	0.612	0.618				0.613
$m = 1$	0.229	0.228				0.231
$m = 2$	0.094	0.090				0.091
$m = 3$	0.038	0.037				0.038
$m = 4$	0.015	0.015				0.015
$m = 5$	0.007	0.006				0.007
% Counting efficiency $n^c = 2$	63.9	59.4				45.7
$n = 3$	58.8	53.3				38.6

<sup>a</sup> Impurity quenching factor (see text).

<sup>b</sup> Note that photons may cross to the other side of the detector.

<sup>c</sup> Only coincident 'pulses' of at least  $n$  photoelectrons are counted.

Table 2 (b). Simulation of the unquenched and impurity situations -  $^{14}\text{C}$ .

	Argon-purged $q^d = 1.0$		Air-quenched $q = 0.75$		Impurity quenched to equivalent of $60 \mu\text{l}$ of $\text{CCl}_4$ in a $20 \text{ ml}$ sample $q = 0.4$	
	All events	Coincident events	All events	Coincident events	All events	Coincident events
Average $\beta$ -energy (keV)	50.2	51.7	49.5	51.4	50.4	53.8
Average number of primary photons	797	821	587	611	319	342
Average number of primary photons trapped due to cylindrical symmetry	282	290	206	214	112	120
Average number of secondary photons	535	551	392	407	213	228
Average number of photons colour quenched by PPO	109	112	80	83	43	46
lost in top absorber	114	117	84	87	45	49
lost in bottom absorber	124	128	91	94	49	52
leaving near side of vial	222	223	165	173	90	95
leaving far side of vial	226	229	166	172	90	96
lost in near side of detector	98	101	73	76	39	42
lost in far side of detector	122	126	90	93	49	52

reaching near photocathode <sup>b</sup>	119	113	92	88	92	48	51
reaching far photocathode <sup>b</sup>	109	112	84	80	84	44	47
Average number of photoelectrons in near photomultiplier	31	32	24	23	24	12	13
in far photomultiplier	28	29	21	20	21	11	12
Average summed 'pulse height'	59	61	45	43	45	23	25
Average lesser 'pulse height'	23	24	18	17	18	9	10
Proportion of photons reaching detector after $m$ re-emissions							
$m = 0$	0.613		0.616				0.615
$m = 1$	0.232		0.230				0.230
$m = 2$	0.092		0.091				0.091
$m = 3$	0.037		0.037				0.037
$m = 4$	0.015		0.015				0.015
$m = 5$	0.007		0.007				0.006
% Counting efficiency $n^c = 2$	96.9		95.9				92.8
$n = 3$	96.4		95.4				91.5

<sup>a</sup> Impurity quenching factor (see text).

<sup>b</sup> Note that photons may cross to the other side of the detector.

<sup>c</sup> Only coincident 'pulses' of at least  $n$  photoelectrons are counted.

Table 3 (a). Simulation of colour quenching —  $^3\text{H}$ .

Colour quenching to an equivalent of $c \mu\text{l}$ of coloured solution <sup>a</sup> in a 20 ml sample						
$c = 20.4$			$c = 73.2$			$c = 162.4$
	All events	Coincident events	All events	Coincident events	All events	Coincident events
Average $\beta$ -energy (keV)	5.7	7.6	5.6	7.8	5.6	8.1
Average number of primary photons	56	77	56	80	56	83
Average number of primary photons trapped due to cylindrical symmetry	19	25	16	23	13	18
Average number of secondary photons	36	48	25	35	21	31
Proportion <sup>b</sup> of photons						
colour quenched by PPO	0.131	0.128	0.091	0.089	0.079	0.077
colour quenched by coloured agent	0.047	0.045	0.250	0.240	0.397	0.384
lost in top absorber	0.132	0.130	0.099	0.100	0.076	0.077
lost in bottom absorber	0.141	0.138	0.107	0.106	0.077	0.076
Average number of photons						
leaving near side of vial	15	20	12	18	9	16
leaving far side of vial	15	21	12	17	10	15

reaching near photomultiplier reaching far photomultiplier	9 7	11 10	7 6	10 9	5 5	9 8
Average number of photoelectrons in near photomultiplier in far photomultiplier	2 1	3 2	1 1	2 2	1 1	2 2
Average summed 'pulse height' Average lesser 'pulse height'	3 1	6 2	2 0	5 1	2 0	4 1
Proportion of photons reaching detector after $m$ re-emissions						
$m = 0$		0.623		0.691		0.721
$m = 1$		0.231		0.214		0.200
$m = 2$		0.087		0.066		0.058
$m = 3$		0.035		0.020		0.016
$m = 4$		0.014		0.006		0.004
$m = 5$		0.006		0.002		0.001
% Counting efficiency $n^c = 2$		57.7		49.9		40.6
$n = 3$		51.8		43.3		33.3

Impurity quenching factor of  $q = 0.75$  used throughout.

<sup>a</sup> See following chapter.

<sup>b</sup> Relative to the number of primary photons.

<sup>c</sup> Only coincident 'pulses' of at least  $n$  photoelectrons are counted.

Table 3 (b). Simulation of colour quenching -  $^{14}\text{C}$ .

Colour quenching to an equivalent of $c \mu\text{l}$ of coloured solution <sup>a</sup> in a 20 ml sample						
	$c = 20.2$		$c = 74.6$		$c = 184.3$	
	All events	Coincident events	All events	Coincident events	All events	Coincident events
Average $\beta$ -energy (keV)	49.1	51.2	48.9	51.3	49.9	53.0
Average number of primary photons	607	633	603	635	618	657
Average number of primary photons trapped due to cylindrical symmetry	206	215	186	196	162	172
Average number of secondary photons	409	427	290	305	241	257
Proportion <sup>b</sup> of photons colour quenched by PPO	0.139	0.138	0.099	0.098	0.080	0.080
colour quenched by coloured agent	0.012	0.011	0.210	0.208	0.360	0.358
lost in top absorber	0.138	0.138	0.108	0.108	0.084	0.084
lost in bottom absorber	0.149	0.149	0.116	0.116	0.087	0.087
Average number of photons leaving near side of vial	171	178	140	148	120	127
leaving far side of vial	171	178	141	142	119	128

reaching near photomultiplier	92	96	79	64	68
reaching far photomultiplier	83	86	72	58	62
Average number of photoelectrons					
in near photomultiplier	23	24	20	16	17
in far photomultiplier	21	22	18	15	16
Average summed 'pulse height'					
Average lesser 'pulse height'	45	47	39	31	33
	17	18	14	10	11
Proportion of photons reaching detector after $m$ re-emissions					
$m = 0$	0.611	0.680		0.719	
$m = 1$	0.233	0.217		0.202	
$m = 2$	0.092	0.079		0.057	
$m = 3$	0.038	0.023		0.016	
$m = 4$	0.016	0.007		0.004	
$m = 5$	0.007	0.003		0.001	
% Counting efficiency $n^c = 2$					
	95.6	94.7		93.4	
$n = 3$					
	94.8	93.8		92.5	

Impurity quenching factor of  $q = 0.75$  used throughout.

<sup>a</sup> See following chapter.

<sup>b</sup> Relative to the number of primary photons.

<sup>c</sup> Only coincident 'pulses' of at least  $n$  photoelectrons are counted.

Table 4. Comparison of simulations of impurity and colour quenching (results are for coincident events only.)

	$^3\text{H}$		$^{14}\text{C}$	
	$q^a = 0.5$	$q = 0.78^b$	$q = 0.4$	$q = 0.78$
Equivalent volume <sup>c</sup> of $\text{CCl}_4$ ( $\mu\text{l}$ )	30	0	60	0
Equivalent volume <sup>c</sup> of coloured agent ( $\mu\text{l}$ )	0	115.6	0	184.3
% Counting efficiency $n^d = 2$	45.7	43.3	92.8	93.4
	$n = 3$	38.6	36.5	91.5
Average $\beta$ -energy (keV)	5.8	5.7	50.4	49.9
Average number of primary photons	36	56	319	618
Proportion of primary photons trapped due to cylindrical symmetry	0.36	0.25	0.35	0.26
Average number of secondary photons	24	22	213	241
Proportion <sup>e</sup> of photons				
colour quenched by PPO	0.136	0.080	0.137	0.080
colour quenched by coloured agent	0	0.370	0	0.360
lost in top absorber	0.144	0.081	0.143	0.084
lost in bottom absorber	0.152	0.085	0.155	0.087
Average number of photons				
leaving near side of vial	10	10	90	120
leaving far side of vial	10	11	90	119
reaching near photomultiplier	6	6	48	64
reaching far photomultiplier	5	6	44	58
Average number of photoelectrons				
in near photomultiplier	1	1	12	16
in far photomultiplier	1	1	11	15
Average summed 'pulse height'	2	2	23	31
Average lesser 'pulse height'	0	0	9	10
Proportion of photons reaching detector after $m$ re-emissions				
$m = 0$	0.613	0.716	0.615	0.719
$m = 1$	0.231	0.204	0.230	0.202
$m = 2$	0.091	0.058	0.091	0.057
$m = 3$	0.038	0.016	0.037	0.016
$m = 4$	0.015	0.004	0.015	0.004
$m = 5$	0.007	0.001	0.006	0.001

<sup>a</sup> Impurity quench factor (see text).<sup>b</sup> Coloured samples were air-quenched.<sup>c</sup> In 20 ml of solution.<sup>d</sup> Only coincident pulses of at least  $n$  photoelectrons are counted.<sup>e</sup> Relative to the number of primary photons.

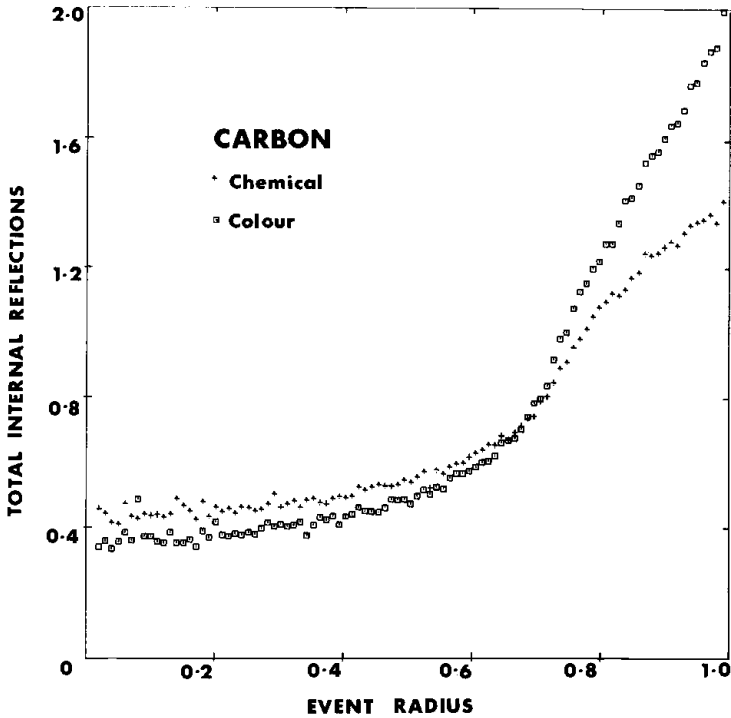


Fig. 4. Light trapping due to the curved walls of the counting vial as a function of the event radius (distance of event from the cylindrical axis) for colour- and chemically quenched  $^{14}\text{C}$  events.

The data therefore show the overall light trapping behaviour of a normal cylindrical vial in relation only to those events enabling coincidence (i.e. counts), and may therefore be regarded as uniformly but conservatively estimating the overall light trapping behaviour in relation to all events (i.e. disintegrations). Note, however, that, although assumed in the model, vials are in practice not perfect cylinders,<sup>4</sup> and therefore that our conservative estimate of light trapping behaviour is more likely to represent the real situation than is an estimate in relation to all events simulated.

There are several points of interest in this behaviour. It can first be seen that, overall, the curves obtained for  $^3\text{H}$  are fuzzier than those for  $^{14}\text{C}$ . A total of 5000  $\beta$ -events was simulated in each of the four cases shown, but  $^3\text{H}$  showed a counting efficiency of only  $\cong 44\%$  by comparison with that of  $\cong 93\%$  obtained for  $^{14}\text{C}$ . Rather fewer data have therefore been included for  $^3\text{H}$ , and those data which have been included derive from the many fewer photons produced during the course of a  $^3\text{H}$  event.

It is, however, more interesting to note that fuzziness increases as radius decreases. This is to be expected because events occur with uniform randomness within the volume of the solution, and therefore about 75% of the events will occur at a radius greater than 0.5 (i.e. proportion of events occurring at radius less than  $r$  is proportional to  $r^2$ ).<sup>6a</sup>

Another feature of Figs. 3 and 4 is that in each case the coloured sample showed more light trapping at higher radii (i.e.  $> \cong 0.7$ ), and less light trapping at lower radii (i.e.  $< \cong 0.7$ ), than its chemically quenched counterpart.

Let us, in considering this behaviour, note first that light trapping at the curved walls of the vial occurs when the angle of incidence, in three dimensions, is greater than the critical angle of the vial-air interface. Now the angle of incidence in three dimensions can be regarded as being composed of horizontal and vertical components, the horizontal one being important in relation to the circular horizontal cross-section of the vial, and the vertical one being important in relation to the rectangular vertical cross-section of the vial and solution.

For photons emitted from points with small radii, the horizontal component of the three-dimensional angle of incidence is largely irrelevant to light trapping behaviour; but, for larger radii, the horizontal component is increasingly influential. A similar argument applies for the vertical component of the angle of incidence; its importance increases as radius increases.

Consider now the overall behaviour at larger radii. In this case, relatively fewer photons will cross to the other side of the vial in a coloured solution, and therefore relatively fewer photons will leave the opposite side of the vial.

Now the horizontal component of the angle of incidence is more important than the vertical one for larger radii, and therefore the total proportion of total internal reflections will be greater in the colour quenching case since:

- (i) photons are more likely to escape via the curved walls of the vial if they have only a short distance to travel through the solution; and
- (ii) those photons travelling a short distance are more likely to have a relatively large horizontal component in their three-dimensional angle of incidence.

The converse situation applies for small radii since the vertical component of the three-dimensional angle of incidence now becomes more important. The total proportion of total internal reflections will now be less in the colour quenching case because:

- (i) photons are more likely to escape via the curved walls of the vial if they have only a short distance to travel through the solution;
- (ii) since the horizontal component of the three-dimensional angle of incidence becomes increasingly irrelevant as radius decreases, those photons taking the shorter paths to the curved walls of the vial and then escaping will be those photons travelling near the horizontal plane; and
- (iii) similarly those photons taking longer paths will tend to have larger vertical components in their three-dimensional angles of incidence, and will thus be more likely to be absorbed before reaching the curved walls of the vial, there to be totally internally reflected.

The chemical- and colour-quenched curves cross at a radius of  $\cong 0.7$ . The significance of this number can be appreciated by noting that, for radii  $< 1/1.474 \cong 0.68$ , the horizontal component of the three-dimensional angle of incidence is always less than the critical angle ( $\sin^{-1} 1/1.474 \cong 43^\circ$ ) for the vial-air interface.

Thus, while the horizontal component becomes increasingly important for higher radii, it plays an increasingly irrelevant role for lower radii, with the cross-over in three dimensions, occurring at a radius of  $\cong 0.7$ .

Clearly, therefore, the light trapping behaviour of the normal LSC system is complicated by its cylindrical symmetry. The seriousness of this light trapping behaviour can be gauged from the improvements in performance observed when cylindrical symmetry is deliberately disrupted by sandblasting the vial's curved outer surface.<sup>21</sup> The authors have proposed elsewhere<sup>5,6b</sup> a spherically symmetrical LSC system of much greater optical efficiency than the cylindrical system, and it should be noted

that spherical systems, by comparison with cylindrical ones, enjoy the invaluable advantage of being much more readily understood.

Consider now the variation of counting efficiency with event radius. Figures 5 and 6 illustrate this behaviour for the simulation of chemically and colour-quenched  $^3\text{H}$  samples of similar counting efficiencies (see Table 4). The area under the data is therefore approximately the same in each case. Note first that fuzziness decreases as radius increases, a situation which is to be expected because events occur at random points within the *volume* of the solution (see above).

Now note that, despite the general fuzziness of the data (20,000 events were simulated in each case), the colour-quenched case shows higher efficiencies at low radii ( $< \cong 0.5$ ) than the chemically quenched case, the converse situation arising to a more marked degree at higher radii ( $> \cong 0.7$ ). The marginally higher efficiencies at low radii for the colour-quenched case are to be expected since light trapping is marginally lower in this case (see Figs. 4, 5). Similarly, the markedly lower counting efficiencies for the colour-quenched sample at higher radii are to be expected since the colour-quenched case shows markedly more light trapping at higher radii (see Figs. 4, 5).

Similar curves have not been presented for  $^{14}\text{C}$  as this isotope shows relatively little departure from a counting efficiency of  $\cong 100\%$ .

Consider, in this last context, Figs. 7 and 8 which show variation of counting efficiency in relation to  $\beta$ -energy for  $^{14}\text{C}$  and  $^3\text{H}$  respectively. Results for simulation runs of chemically and colour-quenched samples are overlaid in each case, with  $^{14}\text{C}$

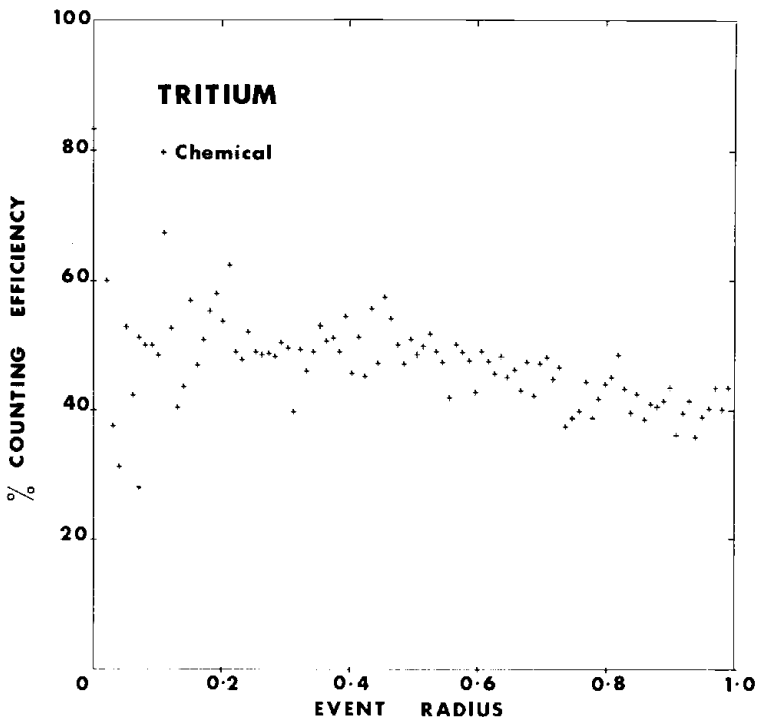


Fig. 5. A plot of average counting efficiency (proportion of events enabling coincidence) for chemically quenched tritium as a function of the event radius (distance of event from the cylindrical axis).

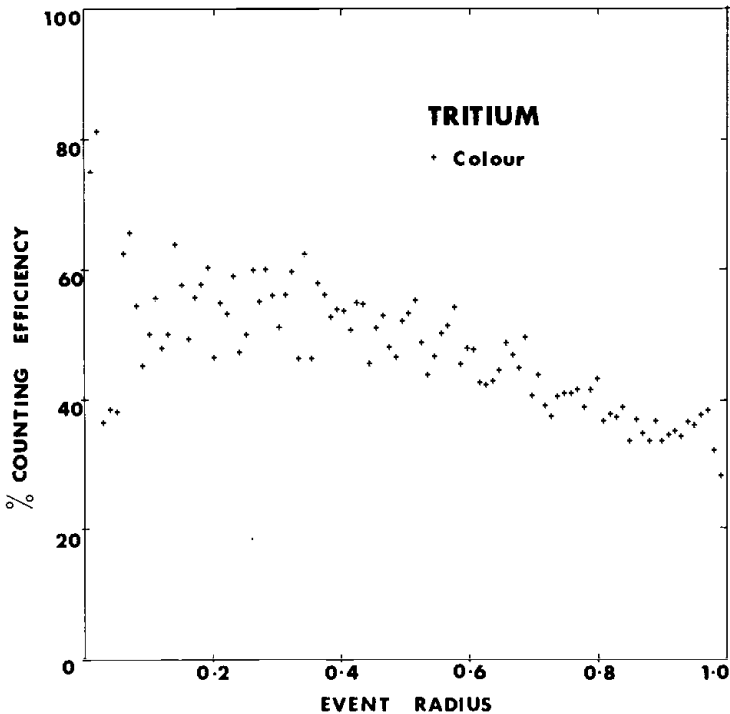


Fig. 6. A plot of average counting efficiency (proportion of events enabling coincidence) for colour-quenched tritium as a function of the event radius (distance of event from the cylindrical axis).

clearly showing a 100% efficiency for almost all events of  $\beta$ -energy greater than about 25 keV (i.e.  $\cong 72\%$  of the  $^{14}\text{C}$   $\beta$ -spectrum; see Table 5).

Counting efficiency gradually decreases below 25 keV, with very similar behaviour being shown for both colour- and chemical-quenching. This is to be expected since:

- (i) only events of low  $\beta$ -energy produce so few photons that, even under quenching conditions, a counting efficiency of 100% is not virtually guaranteed (see Table 1); and
- (ii) because both stochastic simulation runs produced nearly equal overall counting efficiencies the areas under both the chemical- and colour-quenched curves must be approximately the same.

Figure 8 illustrates the counting efficiency/energy relationship for  $^3\text{H}$ , and demonstrates more effectively how counting efficiency increases with  $\beta$ -energy in the low range. The relationship is sigmoid and clearly not simple, this being expected since the scintillation efficiency  $S_E$  is an increasing but non-linear function of  $\beta$ -energy.

Another feature of interest in Fig. 8 is that fuzziness increases with  $\beta$ -energy. This situation is to be expected since the  $^3\text{H}$   $\beta$ -energy spectrum falls off sharply as  $\beta$ -energy increases, with correspondingly fewer  $\beta$ -events being produced with these energies (see Table 5).

Let us now consider the digital 'pulse height spectra' produced by the model. There are two different approaches to pulse height analysis in LSC, the first and more traditional method being to combine the analogue pulses from each photomultiplier for those events in which coincidence is enabled. This 'summed' pulse then charac-

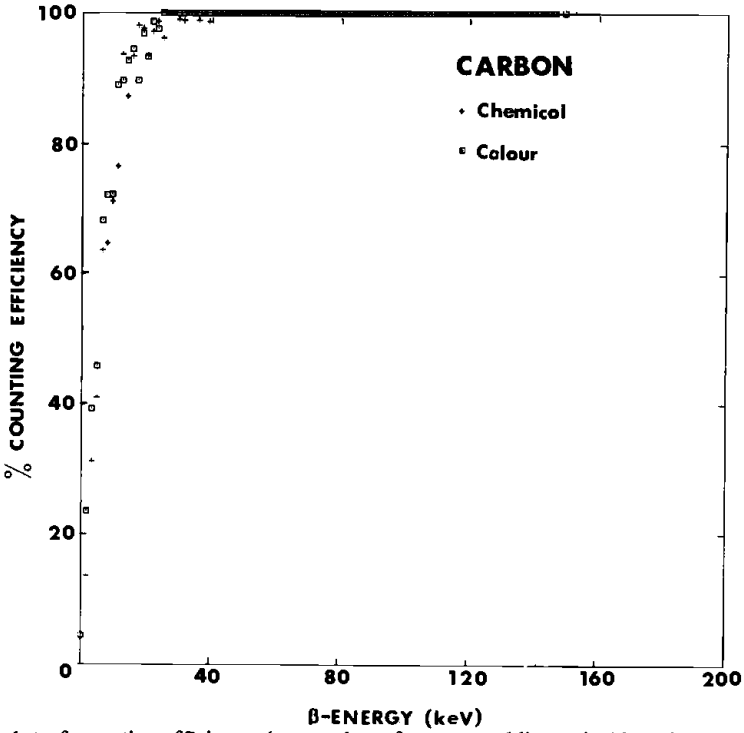


Fig. 7. A plot of counting efficiency (proportion of events enabling coincidence) versus  $\beta$ -energy for colour- and chemically quenched  $^{14}\text{C}$  events (integral counting efficiency  $\cong 93\%$ ).

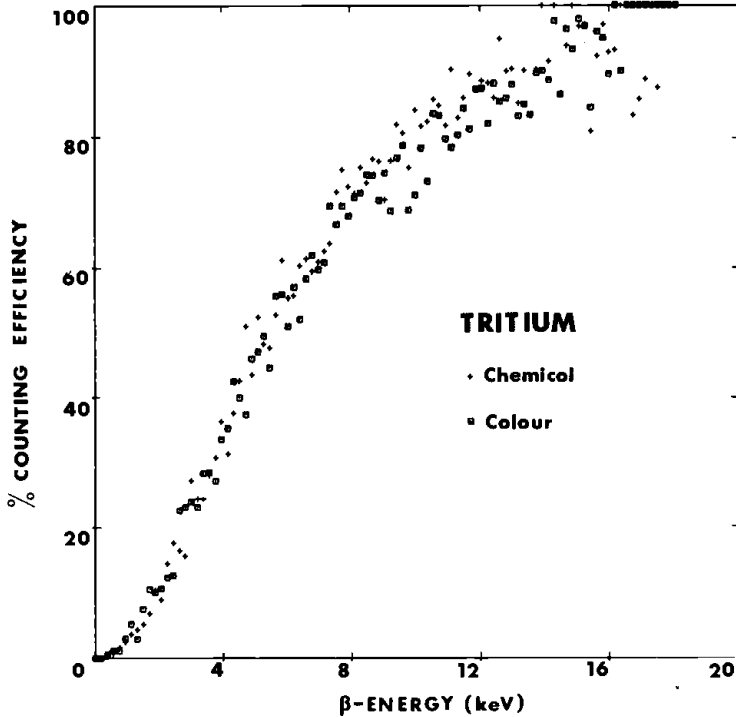


Fig. 8. A plot of counting efficiency (proportion of events enabling coincidence) versus  $\beta$ -energy for colour- and chemically quenched  $^3\text{H}$  events (integral counting efficiency  $\cong 44\%$ ).

Table 5. Fermi distribution<sup>6a</sup> of energies of  $\beta$ -particles emitted by  $^3\text{H}$  and  $^{14}\text{C}$ .

$^3\text{H}$		$^{14}\text{C}$	
$\beta$ -energy $e$ (keV)	% of $\beta$ -particles emitted with an energy $> e$	$\beta$ -energy $e$ (keV)	% of $\beta$ -particles emitted with an energy $> e$
1.0	91.1	10	89.6
2.0	81.1	20	78.1
3.0	70.8	30	66.4
4.0	60.7	40	55.1
5.0	51.1	50	44.5
6.0	42.2	60	34.8
7.0	34.1	70	26.3
8.0	26.8	80	19.0
9.0	20.5	90	13.0
10.0	15.2	100	8.3
11.0	10.8	110	4.8
12.0	7.2	120	2.4
13.0	4.5	130	0.9
14.0	2.6	140	0.2
15.0	1.3	150	0.01
16.0	0.5		
17.0	0.1		
18.0	0.01		

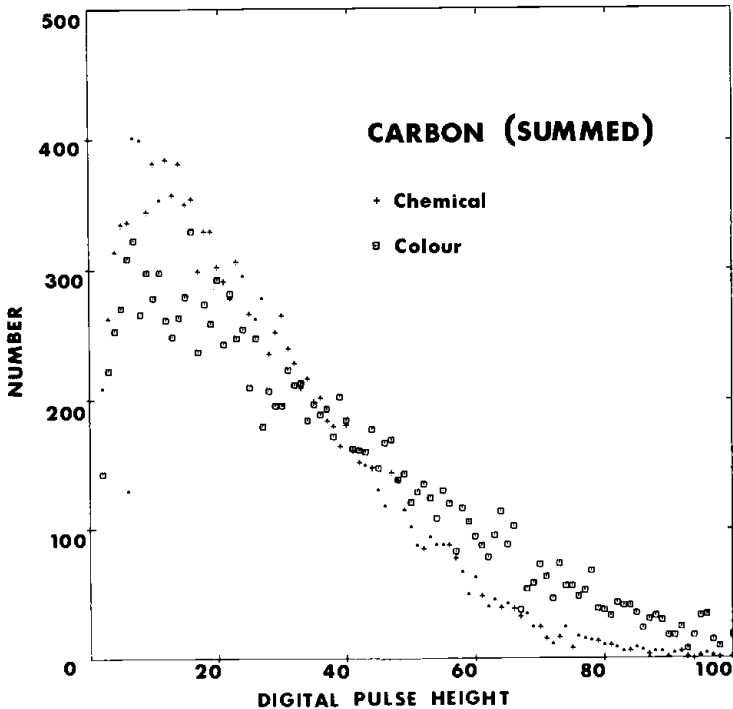


Fig. 9. A digital summed pulse height spectrum for colour- and chemically quenched  $^{14}\text{C}$  events enabling coincidence. Integral counting efficiency  $\cong 93\%$  in each case. (Note the different vertical scale when compared to Fig. 10.)

terises that (coincident) event, and is further analysed according to discriminator settings, etc. Figure 9 shows digital summed pulse height spectra obtained with the model for colour- and chemically quenched  $^{14}\text{C}$  samples counted with similar efficiencies. 15,000 events were simulated in each case.

The second method, known as 'lesser' pulse height analysis, is due to a penetrating insight by Laney.<sup>18,19</sup> The approach in this case is to analyse only the smaller or lesser of the two pulses arising in photomultipliers for coincident events.

Thus, in that only those pulses are analysed which arise from events enabling coincidence, the lesser approach is therefore identical to the traditional one. The difference from the traditional approach arises after coincidence is enabled; whereas the 'summed' method combines the pulses from both photomultipliers, the 'lesser' method, when applied in its pure form, analyses only the smaller of the two pulses from the photomultipliers, the larger pulse being discarded.

Clearly, therefore, the summed and lesser methods will in practice show no difference for counting efficiency in an integral counting window since, in this case, counting efficiency is given by (number of coincident events)/(number of dis-integrations or events).

Figure 10 shows the digital lesser pulse height spectra resulting from the same two simulation runs, each of 15,000 events, that produced the data for Fig. 9; the spectra produced in each case are therefore comparable. Figure 9 clearly illustrates the behaviour observed in practice (see, for example, Fig. 9 of Ref. 19) for colour- and chemically quenched samples. The spectrum of the coloured sample has a lower maximum value and a longer 'tail' than its chemically quenched counterpart.

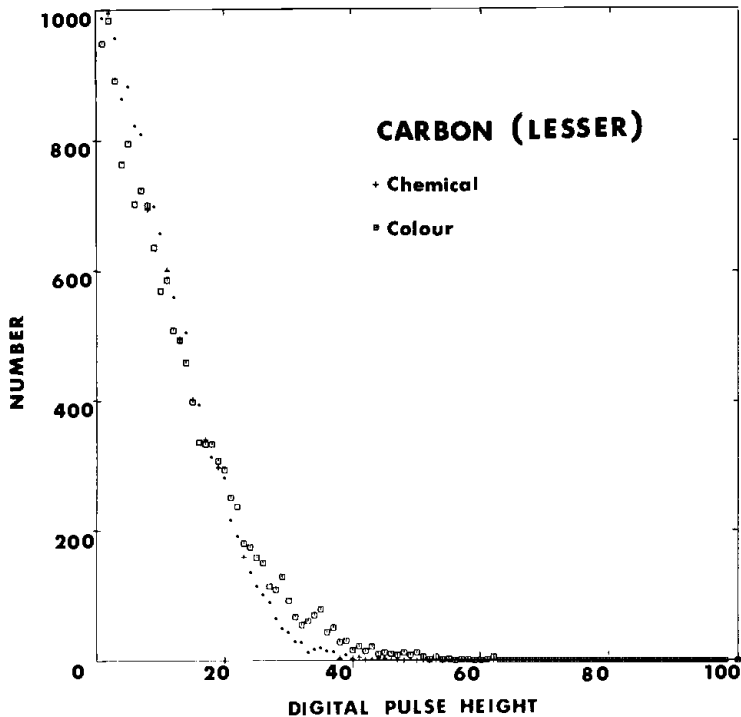


Fig. 10. A digital lesser pulse height spectrum for colour- and chemically quenched  $^{14}\text{C}$  events. Integral counting efficiency  $\cong 93\%$  in each case. (Note the different vertical scale when compared to Fig. 9.)

This trend is, as expected (see Fig. 9 of Ref. 19), present to a markedly smaller degree in the lesser spectra (see Fig. 10). The behaviour of the model is therefore consistent with the spectra produced in practice for both the summed and lesser systems.

## CONCLUSIONS

The above model offers a useful understanding of some of the more essential of the complicated interactions constituting the LSC process as it occurs in practice. While it is clear that definitive accuracy is still lacking in many of the data (e.g. scintillation efficiency and detector response), and other important data are missing (e.g. pulse spread and losses along the dynode string of the photomultipliers in our instruments), the model's behaviour is nonetheless in accordance with that observed in the laboratory. Note that the more practical implications of this study are contained in the following chapter.

## ACKNOWLEDGEMENTS

Grateful thanks are given to the Staff of the Computing Centre of the University of Adelaide, without whose assistance this study would have been impossible. We are also indebted to Dr. John Birks, Dr. Donald Horrocks, Mr. Philip Kreveld, Mr. Donald Moore and Mr. Edward Polic for providing invaluable numerical data and advice. Finally we thank Mrs Ermioni Mourtzios and Mrs Helen Simpson for preparing the manuscripts.

## REFERENCES

1. J. B. Birks, *The Theory and Practice of Scintillation Counting*, Pergamon, London, 1964.
2. E. Rapkin, *Laboratory Scintillator* 11 (October 1966).
3. L. A. Baillie, *Intern. J. Appl. Radn. Isotopes* 8, 1-7 (1960).
4. P. E. Stanley and P. J. Malcolm, 'Practical liquid scintillation spectrometry: organising a methodology', this volume, pp. 44-62.
5. P. J. Malcolm and P. E. Stanley, 'Low level counting using liquid scintillation spectrometry: optimizing optical design', paper to be published in the proceedings of an *International Conference on Low Radioactivity Measurements and Applications*, High Tatras, Czechoslovakia, October 1975, Comenius University Press, Czechoslovakia.
- 6a. P. J. Malcolm and P. E. Stanley, A unified approach to the liquid scintillation counting process: Part I, A stochastic computer model, *Intern. J. Appl. Radn. Isotopes* (in press).
- 6b. P. J. Malcolm and P. E. Stanley, A unified approach to the liquid scintillation counting process: Part II, Optimizing optical design, *Intern. J. Appl. Radn. Isotopes* (in press).
7. P. J. Malcolm and P. E. Stanley in *Liquid Scintillation Counting: Recent Developments* (eds. P. E. Stanley and B. A. Scoggins), Academic Press, New York, 1974, pp. 77-90.
8. F. E. L. ten Haaf in *Liquid Scintillation Counting*, Vol. 2 (eds. M. A. Crook, P. Johnson and B. Scales), Heyden, London, 1972, pp. 39-48.
9. F. E. L. ten Haaf in *Liquid Scintillation Counting*, Vol. 3 (eds. M. A. Crook and P. Johnson), Heyden, London, 1974, pp. 41-6.
10. F. E. L. ten Haaf and M. L. Verheyke, 'A simple mathematical model of a liquid scintillation counter', this volume, pp. 63-73.
11. M. P. Neary and A. L. Budd in *The Current Status of Liquid Scintillation Counting* (ed. E. D. Bransome), Grune and Stratton, New York, 1970, pp. 273-82.

12. N. Kaczmarczyk in *Organic Scintillators and Liquid Scintillation Counting* (eds. D. L. Horrocks and C-T Peng), Academic Press, New York, 1971, pp. 977-90.
13. D. L. Horrocks, *Applications of Liquid Scintillation Counting*, Academic Press, New York, 1974.
14. D. L. Horrocks in *Liquid Scintillation Counting*, Vol. 3 (eds. M. A. Crook and P. Johnson), Heyden, London, 1974, pp. 1-20.
15. D. L. Horrocks, personal communication.
16. D. Moore, personal communication.
17. J. B. Birks, personal communication.
18. B. H. Laney in *Liquid Scintillation Counting: Recent Developments* (eds. P. E. Stanley and B. A. Scoggins), Academic Press, New York, 1974, pp. 455-64.
19. C. Ediss, A. A. Noujaim and L. J. Wiebe in *Liquid Scintillation Counting: Recent Developments* (eds. P. E. Stanley and B. A. Scoggins), Academic Press, New York, 1974, pp. 91-111.
20. E. Rapkin in *Liquid Scintillation Counting*, Vol. 2 (eds. M. A. Crook, P. Johnson and B. Scales), Heyden, London, 1972, pp. 61-100.
21. B. E. Gordon and R. M. Curtis, *Anal. Chem.* **40**, 1486-93 (1968).

## DISCUSSION

For discussion relating to this chapter, see p. 62.

(Copyright reserved)